Thin Solid Films 518 (2010) 1839–1849

Contents lists available at ScienceDirect

Thin Solid Films

journal homepage: www.elsevier.com/locate/tsf

Review

High mobility transparent conducting oxides for thin film solar cells

S. Calnan [a,*], A.N. Tiwari [b]

[a] Centre for Renewable Energy Systems Technology, Department of Electronic and Electrical Engineering, Loughborough University, Leicestershire, LE11 3TU, UK
[b] Laboratory for Thin Films and Photovoltaics, Swiss Federal Laboratories for Materials Testing and Research (EMPA), Überlandstr, 129, CH-8600 Dübendorf, Switzerland

ARTICLE INFO

Available online 19 September 2009

Keywords:
Transparent conducting oxide
High mobility
Solar cells

ABSTRACT

A special class of transparent conducting oxides (TCO) with high mobility of $>65\ cm^2V^{-1}s^{-1}$ allows film resistivity in the low $10^{-4}\Omega cm$ range and a high transparency of >80% over a wide spectrum, from 300 nm to beyond 1500 nm. This exceptional coincidence of desirable optical and electrical properties provides opportunities to improve the performance of opto-electronic devices and opens possibilities for new applications. Strategies to attain high mobility (HM) TCO materials as well as the current status of such materials based on indium and cadmium containing oxides are presented. Various concepts used to understand the underlying mechanisms for high mobility in HMTCO films are discussed. Examples of HMTCO layers used as transparent electrodes in thin film solar cells are used to illustrate possible improvements in solar cell performance. Finally, challenges and prospects for further development of HMTCO materials are discussed.

Contents

* Corresponding author. Present address: Helmholtz Zentrum Berlin für Materialien und Energie GmbH, PVcomB, Schwarzschildstrasse 3, D-12489, Berlin, Germany.
E-mail address: sonya.calnan@helmholtz-berlin.de (S. Calnan).

0040-6090/$ – see front matter
doi:10.1016/j.tsf.2009.09.044

1. Introduction

Transparent conducting oxide (TCO) layers are characteristically described as thin films that exhibit simultaneously high visible wavelength transparency and electrical conductivity. The majority of known TCO materials are n-type semiconductors where defects such as oxygen vacancies, impurity substitutions and interstitials donate electrons to the conduction band providing charge carriers for the flow of electric current [1]. However, hole doping by ionised cation vacancies, impurity acceptor ion substitutions and/or oxygen interstitials which act as electron acceptors is also possible leading to p-type TCO materials [2]. Although p-type TCO materials have been reported, the commonly applied TCO materials are n-type semiconductors namely, F- or Sb-doped tin oxide, Sn- or Zn-doped indium oxide and Al-, B- or Ga-doped zinc oxide. These films are used in low emissivity windows, gas sensors, flat panel displays, thin film transistors, light emitting diodes and solar cells, to name a few [1,3–7]. Significant progress has been made in optimising the preparation of TCO thin films for large area depositions required by industry such as increasing the deposition rate, low temperature processing on plastic substrates and improvement of uniformity, among others. However, the resistivity of these films has saturated at about $10^{-4}\,\Omega$cm though values in the range of $10^{-5}\,\Omega$cm can be obtained under controlled laboratory conditions [7]. Other well known TCO materials are In- or Sn-doped CdO which are not widely used because of the hazardous nature of cadmium and a negative public perception against cadmium containing compounds.

The resistivity ρ, of a semiconductor is related to the charge carrier density N and the carrier mobility μ by the relation

$$\frac{1}{\rho} = N\mu e \tag{1}$$

where e is the electronic charge given by 1.602×10^{-19}C. If N is increased to reduce ρ, the TCO film transmission especially in the near infrared (NIR) region reduces as a result of absorption by free carriers or by metal-like reflection. It is therefore, important that further reductions in the TCO resistivity must not adversely reduce the optical transparency of the film. However ρ of a TCO film may be decreased without reducing the NIR transmission by increasing μ rather than N. Fig. 1 shows the evolution of absorptance in a material with a fixed carrier density ($5\times10^{20}\,\mathrm{cm}^{-3}$) as the mobility increases [8].

Since TCO films useful for most applications must have a wide band gap (>3.0 eV) which requires a degenerate carrier density $\geq10^{20}\,\mathrm{cm}^{-3}$ and ideally $\rho<10^{-3}\,\Omega$cm, using Eq. (1), the corresponding Hall mobility would be $\mu\geq62.5\,\mathrm{cm}^2\mathrm{V}^{-1}\mathrm{s}^{-1}$. Therefore, in this contribution, high mobility transparent conducting oxides (HMTCO) are used to refer to TCO films which fulfill the above conditions and have a value of mobility $\geq62.5\,\mathrm{cm}^2\mathrm{V}^{-1}\mathrm{s}^{-1}$. Ti- and Mo-doped In_2O_3 (in short, ITiO and IMO respectively) are examples of TCO materials possessing high mobility $>62.5\,\mathrm{cm}^2\mathrm{V}^{-1}\mathrm{s}^{-1}$ with high NIR transparency while maintaining low $\rho\sim10^{-4}\,\Omega$cm. Fig. 2 shows the transmission and reflection spectra of several thin films composed of ITiO, IMO, In_2O_3:Sn (ITO) and SnO_2:F (FTO). The ITiO and IMO films were prepared by magnetron sputtering in research laboratory conditions while the ITO and FTO films were obtained from commercial vendors, for details refer to a previous study in [9]. The sheet resistance of the films ranges from 6 Ω/□ to 11 Ω/□ and the indium based films have a comparable resistivity $\rho<2\times10^{-4}\,\Omega$cm while that of the FTO film is slightly higher at $3.9\times10^{-4}\,\Omega$cm. While the transmission of the ITO film begins to dip at around 950 nm, that of the IMO and ITiO films remains high and begins to dip for wavelengths >1200 nm. Though the NIR optical loses may be further reduced by reducing N, doing so indiscriminately can decrease the conductivity and/or the optical band gap of the TCO layer and adversely affect the electrical properties and transparency in the visible wavelength region. Therefore, TCO materials with sufficiently high N ($\geq10^{20}\,\mathrm{cm}^{-3}$) while maintaining a high mobility and transparency are desirable. High mobility TCO materials have been prepared in the past but the resistivity has been greater than $10^{-3}\,\Omega$cm because of a relatively low $N<10^{19}\,\mathrm{cm}^{-3}$ [10,11]. Such low carrier density levels would require a Hall mobility in the excess of $400\,\mathrm{cm}^2\mathrm{V}^{-1}\mathrm{s}^{-1}$ to achieve $\rho<10^{-4}\,\Omega$cm. CdO is a well known material with mobility as high as $\mu=146\,\mathrm{cm}^2\mathrm{V}^{-1}\mathrm{s}^{-1}$ with $N=1.5\times10^{20}\,\mathrm{cm}^{-3}$ [12] but is not suitable for most TCO applications because of absorption in the visible light spectrum as a result of a low band gap <3.0 eV and environmental issues.

High mobility TCO films with a sheet resistance of ≤10 Ω/□ and an optical transmission of ≥80% over the visible to NIR wavelengths are potentially useful to enhance solar cell efficiency. This is particularly useful in the case of multi-junction solar cells, consisting of stacks of different semiconductors with appropriately matched band gaps to increase the spectral response over a wide wavelength range. Ideally, the bottommost cell should receive photons that are unused by the upper absorbers and thus transmitted through the upper cells including their TCO contacts. Fig. 3 shows a graph comparing the external quantum efficiency (EQE) of single junction solar cells based on absorbers with different optical band gaps and using conventional TCO materials such as ZnO:Al and In_2O_3:Sn as transparent contacts. The EQE curve of the gallium rich $CuIn_{1-x}Ga_xSe_2$ (CIGS) cell, labelled C, in Fig. 3 is unexpectedly low for energies above the theoretical band gap because of poor current collection as a result of recombination [13]. Otherwise, for all the solar cells, a significant portion of the loss in EQE is caused by optical losses in the front contact TCO. If such solar cell structures are used in a multi-junction device, the amount of light reaching the bottom absorber (with the lowest band gap) is severely reduced causing a current mismatch [14]. When comparing the EQE of the CIS absorber represented by curve A in Fig. 3 with the TCO transmission spectra presented in Fig. 2, it is clear that improvements in the EQE, especially for wavelengths greater than 900 nm are possible if HMTCO contacts are used. Thus, HMTCO films could potentially improve the efficiency of such solar cells by reducing the optical losses while minimising resistive losses.

In this article strategies used to improve the carrier mobility in degenerately doped TCO thin films are reviewed. A survey of dopant elements known to improve the mobility of In_2O_3 and CdO is presented. A discussion aimed at understanding the reasons for high mobility in these materials is given. Examples of the application of HMTCO films in solar cells are described and used to illustrate the potential benefits of improved NIR transmission to these devices. Finally, challenges and prospects for further development of HMTCO materials are discussed.

2. Strategies to attain high mobility in TCO materials

Various strategies have been employed to increase the mobility of TCO thin films while maintaining high transparency and conductivity as reviewed by Exarhos and Zhou [15]. Traditionally, the mobility of TCO thin films has been enhanced by improving the crystalline structure by means such as heat treatment, choice of deposition technique as well as choice of substrate. Here, we expand on some of those strategies and include several other methods that are perhaps less well known, but seem promising.

2.1. Post deposition heat treatment

TCO thin films prepared without intentional substrate heating or with low process temperatures exhibit low electron mobility as a result of scattering by grain boundaries and/or point defects. Post deposition heat treatment in different ambient conditions reduces point and/or dislocation defects in the amorphous or poorly crystallised TCO films by increasing the grain size and improving the overall crystal structure enhancing the electron mobility [3,16]. However, effective heat treatment may require temperatures approaching

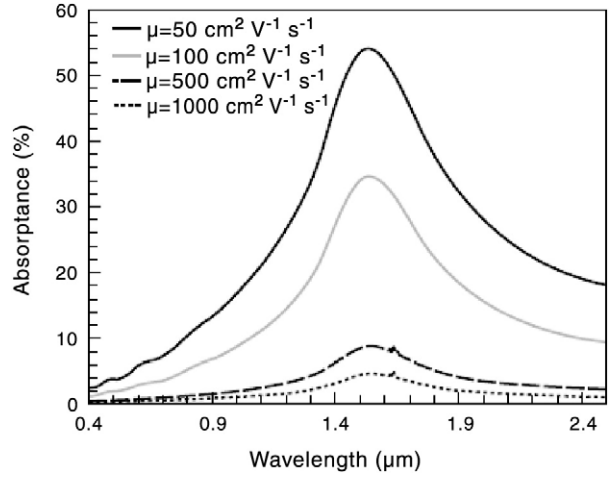

Fig. 1. Variation of absorptance with wavelength for TCO films with constant carrier density but varying mobility. The absorptance was modelled using Drude's theory. Reproduced by permission of the MRS Bulletin [8].

600 °C, that are unsuitable for heat sensitive substrates such as polymers or even soda lime glass which may soften and introduce undesirable impurities in the TCO films and thus other methods have to be used.

2.2. Choice of deposition method

While film growth by highly energetic particles may increase the grain size of TCO films, an excessive transfer of momentum may damage the films and reduce the mobility [16]. During sputtering, the discharge voltage at the target surface repels both negative oxygen ions and neutral argon atoms, which arrive at the substrate with high kinetic energy of ~100 eV and distort the TCO crystalline structure [17]. Since the discharge voltage is less for RF sputtering than for DC sputtering, it is usual for TCO films grown by the former method to have higher values of mobility [17,18]. The kinetic energy of particles related to pulsed laser deposition varies from 1 eV to a few 100 eV but is easier to control than in sputtering resulting in better TCO crystalline structures leading to higher mobility [19].

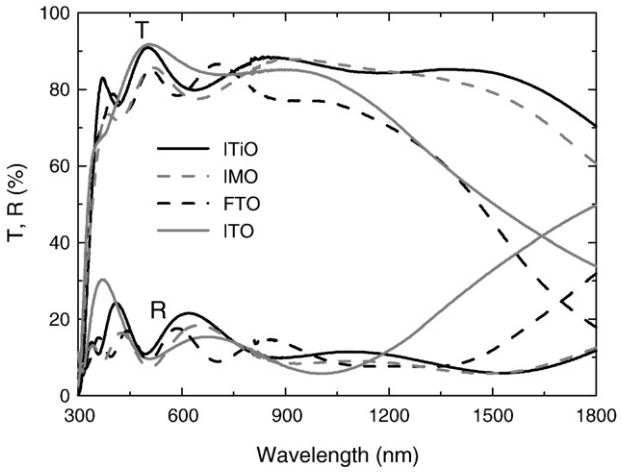

Fig. 2. Transmission T and reflection R spectra of ITiO, IMO, ITO and FTO thin films on 1.1 mm soda lime glass. The mobility values are 105 $cm^2V^{-1}s^{-1}$, 77 $cm^2V^{-1}s^{-1}$, 27 $cm^2V^{-1}s^{-1}$ and 25 $cm^2V^{-1}s^{-1}$ for ITiO, IMO, ITO and FTO, respectively. The resistivity values of the indium based films range from $1.3\times10^{-4}\,\Omega$cm to $1.9\times10^{-4}\,\Omega$cm while that of the FTO film is $3.9\times10^{-4}\,\Omega$cm. Reproduced with permission from [9].

2.3. Control of crystal structure using mono-crystalline substrates

Control of crystal growth by using highly oriented substrates is known to enhance the mobility of TCO thin films by improving crystallinity. Yttria-stabilized zirconia (100) is often used to grow low resistivity ITO thin films [20]. Though the ITO crystal quality can be improved the increase in the mobility is not drastic compared to ITO prepared on glass. Therefore, other factors such as the character of the doping ions may play a role in determining the charge carrier mobility. However, the highest reported mobility for highly conductive ZnO:Al ~ 70 $cm^2V^{-1}s^{-1}$ at $N > 10^{20}\,cm^{-3}$ has been reported for films grown on c-plane sapphire [19]. A study of Cd_2SnO_4 films grown on different substrate illustrates this point further where the mobility of the films was measured as 609 $cm^2V^{-1}s^{-1}$ (the highest reported value for a degenerate TCO material), 330 $cm^2V^{-1}s^{-1}$ and 27 $cm^2V^{-1}s^{-1}$ using MgO(111), MgO(100) and boro-silicate glass substrates, respectively [21]. The relatively high cost and limited suitability of these highly oriented substrates on large areas precludes the use of epitaxially grown TCO in a wide range of applications, especially displays and solar cells.

2.4. Controlling impurity concentration

Hall mobility in TCO thin films can be increased by reducing scattering caused by intrinsic crystalline defects and/or ionised impurities. A relatively high mobility in ZnO:Al up to 44.2 $cm^2V^{-1}s^{-1}$ with $N = 3.8\times10^{20}\,cm^{-3}$ was achieved using a ZnO target with a low Al_2O_3 concentration of 0.5 wt.% [22]. By minimising intrinsic defects in thin film ZnO, a mobility of 440 $cm^2V^{-1}s^{-1}$ but with a low N of $< 10^{16}\,cm^{-3}$ could be achieved [11].

2.5. Selective doping methods

Selective doping methods may increase the relaxation time in TCO materials by separating the doping and charge transport regions. In such cases, the charge carriers are provided by the heavily doped regions while the lightly doped regions provide a high mobility path where scattering by ionised or neutral impurities, is minimised. Zone confining is achieved by applying a (quasi) periodic temperature gradient across the surface of the substrate during deposition of the TCO material [23].

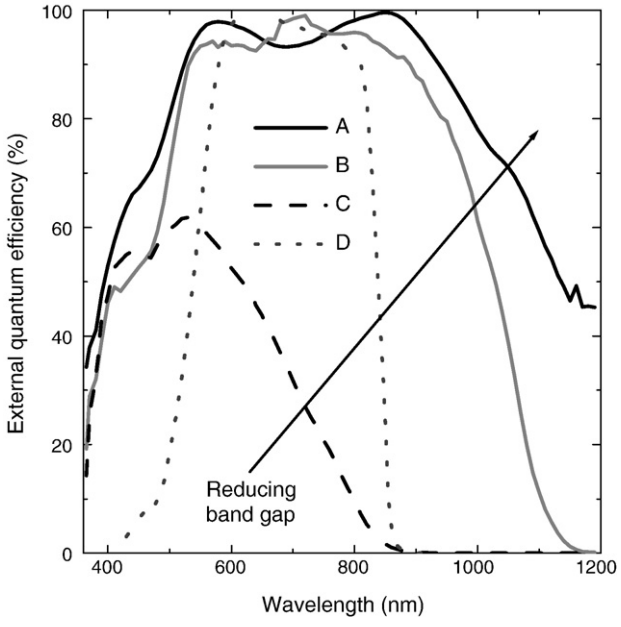

Fig. 3. External quantum efficiency spectra of solar cells based on absorber materials with varying optical energy band gap where A is CIS, B is CIGS with (Ga/(Ga + In) = 0.3), C is CIGS with (Ga/(Ga + In) = 0.8) and D is CdTe.

During film growth, the impurities tend to accumulate in the colder areas of the substrate surface. The impurity movement and temperature gradient are mutually parallel and are perpendicular to the growth direction. The result is a film consisting of alternate zones of heavily doped metal oxide and almost pure metal oxide (see Fig. 4a). Using this method, a high mobility of 103 $cm^2V^{-1}s^{-1}$ and an average carrier density of $1.4\times10^{21}cm^{-3}$ give a resistivity of $4.4\times10^{-5}\Omega$ cm for ITO [23,24]. However, the visible transparency of ITO prepared using this method including the substrate, was below 80% [24].

Selective doping using multi-layered films composed of lightly and heavily doped semiconductors alternately stacked in the direction of the film growth (see Fig. 4b), is also referred to as modulation doping [25]. Several studies predict that modulation doping may improve TCO mobility [26,27]. Simulations on multi-layered films composed of $InGaO_3$ (relatively large electron affinity and low carrier density) alternately stacked with ZnO:Al layers (low electron affinity and high carrier density) have predicted that high conductivity $>4.2\times10^4$ S cm^{-1} for carrier densities $\sim10^{20}cm^{-3}$ are possible [26]. Simulations of the transport mechanisms revealed that the conductivity is very sensitive to the quantum well thickness. The authors proposed that high mobilities derived from doping modulation would require individual layers of <5 nm thick and high crystal quality materials with close lattice matching in order to avoid interface defects which would be challenging to achieve in practice [26]. A mobility of 1560 cm $V^{-1}s^{-1}$ is possible if $N=1\times10^{20}cm^{-3}$ at the bottom of a 5 nm wide quantum well giving a resistivity of $4.0\times10^{-5}\Omega$ cm. A similar simulation was performed for modulation-doped multi-layers composed of ZnO|ZnMgO|ZnMgO:Al|ZnMgO all of which are closely lattice matched [26]. Mobilities as high as 145 $cm^2V^{-1}s^{-1}$ were predicted for a structure with an average carrier density of $3.8\times10^{18}cm^{-3}$ but the lowest resistivity was limited to $1.5\times10^{-3}\Omega$ cm. Multi-layers consisting of ZnO|ZnO:Al and ZnO|$Zn_{1-X}Mg_XO$:Al have also been prepared on a- and c-plane sapphire substrates and though the crystal structure was comparable to that of single layers, the resistivity was quite high [28]. The authors attributed this effect to the high oxidation sensitivity of the thin films which passivated the donors and reduced the carrier density. Also, multi-layered films consisting of the dopant oxide films alternating with the host cation oxide have been prepared, i.e. InO_X (2.0 nm)|SnO_Y (0.2 nm) obtaining a relatively low mobility of 17 $cm^2V^{-1}s^{-1}$ and a carrier density of $5\times10^{20}cm^{-3}$ [29]. To date, the predicted high mobility cannot be obtained in thin films prepared by modulation doping as desired for most TCO applications such as photovoltaic cells.

2.6. Hydrogen inclusion

Total energy calculations based on first principles suggest that the bond length between hydrogen and the nearest host oxygen atom in a metal oxide is virtually the same regardless of the metal [30]. Therefore, the hydrogen is "pinned" at a fixed energy level which introduces shallow defect states inside the conduction band of oxides with a high electron affinity leading to n-type doping. It has also been suggested that hydrogen passivates structural defects in TCO materials in the same way as is well known for thin film silicon [31,32]. Hydrogen inclusion in TCO materials is achieved either during film deposition or by post deposition annealing in a hydrogen atmosphere. One of the highest mobilities for ITO ($\mu\sim145$ $cm^2V^{-1}s^{-1}$ for $N>10^{20}cm^{-3}$) has been achieved by post deposition treatment in a hydrogen plasma [32] while that for ZnO:Al ($\mu\sim50$ $cm^2V^{-1}s^{-1}$ for $N>10^{20}cm^{-3}$) has been reported for films sputtered with a small amount of hydrogen added to the sputter gas [33]. A high value of $\mu=130$ $cm^2V^{-1}s^{-1}$ for $N=1.8\times10^{20}cm^{-3}$ has also been reported for hydrogen doped In_2O_3 [32].

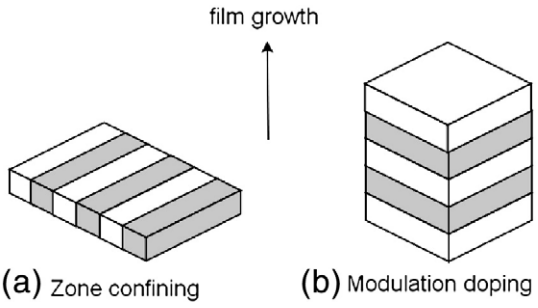

Fig. 4. Schematic showing charge carrier distributions in relation to the direction of film growth of semiconductors prepared using selective doping by zone confining (a) and modulation (b). The dark and light sections denote regions of high and low carrier density, respectively.

2.7. Choice of appropriate dopants

The highest mobilities achieved for conventional degenerate TCO thin films prepared by sputtering are typically 40–50 $cm^2V^{-1}s^{-1}$ for ITO [16,34,35] and ZnO:Al [7,17]. However, specific elements have been used to prepare degenerate CdO and In_2O_3 thin films by sputtering with $\mu>62.5$ $cm^2V^{-1}s^{-1}$ with transmission of $>80\%$ in the visible and near infra-red wavelength regions. While undoped CdO thin films have a high mobility, the optical band gap is too low for use as a transparent conductor for visible light. However, doping cadmium oxide with several elements e.g. In [12], Sc [36], Y [37] and Ti [38] can lead to mobilities above 62.5 $cm^2V^{-1}s^{-1}$ while maintaining $N\geq10^{20}cm^{-3}$. A wider range of doping elements has been used to achieve high mobility in In_2O_3 thin films such as Mo [39–41], Ti [42–47], W [48–51], Zr [42,43,52–55], and Gd [56]. Details of dopants elements leading to high mobility in CdO and In_2O_3 are presented later in Section 4.3.

3. Deposition methods for degenerate TCO thin films with mobility higher than 62 $cm^2V^{-1}s^{-1}$

Impurity doped In_2O_3 thin films with high mobility can be prepared using a variety of methods as listed in Table 1. It is apparent from Table 1 that though high mobility in impurity doped In_2O_3 can be achieved by a wide range of deposition techniques, the use of pulsed laser deposition (PLD) and/or post deposition annealing further enhances the Hall mobility. The lowest resistivity reported for IMO thin films to date is $6.7\times10^{-5}\Omega$ cm with a high mobility (250 $cm^2V^{-1}s^{-1}$) grown at 500 °C by PLD on quartz [41]. However, the NIR optical transmission is not known as a high transmittance (~90%) was only presented for visible light.

4. Understanding the mechanisms of high mobility in impurity doped CdO and In_2O_3

The mobility μ of an electron in semiconductors depends on the relaxation time τ, the electronic charge e and the effective carrier mass m^* in the conduction band as given by the following relationship

$$\mu = \frac{e\tau}{m^*}. \quad (2)$$

Therefore, the mobility can be increased by increasing τ or by decreasing m^*. Increasing τ requires films with fewer defects which may be achieved by lower carrier density, less grain boundaries and less neutral impurities. Decreasing m^*, requires semiconductors with a widely dispersed conduction band.

The scattering mechanisms that govern the electron transport in semiconductors are described in detail in text books such as that by Lundstrom [64]. Of these, the scattering mechanisms relevant to n-type TCO thin films have been identified by other authors [3,65–67]. Briefly, they are:

i. Grain boundary scattering caused by the discontinuity presented by grain boundaries especially in polycrystalline thin film

materials. A space charge region formed around the grain boundaries and the resulting potential barrier scatters the electrons crossing this region reducing the mobility. Grain boundary scattering only significantly affects the overall TCO mobility if the grain size is about the same as the mean free path of the charge carriers.

ii. Ionised impurity scattering caused by deflection of free carriers by the long-range electrostatic fields associated with intentional dopants and defects such as interstitials and vacancies.

iii. Optical phonon scattering caused by lattice vibrations of bonds in a polar semiconductor which induce an electric field that interacts with a charge moving through the lattice.

iv. Acoustic-phonon scattering caused by an acoustic wave propagation through a crystal lattice which causes the atoms to oscillate about their equilibrium positions and interfere with the electron motion.

v. Neutral impurity scattering caused by non-ionised impurities.

vi. Piezoelectric scattering which arises from electric fields caused by the strain associated with lattice vibrations in crystals where partially ionic bonds occur such that the unit cell does not contain a centre of symmetry.

Matthiesen's rule states that the contribution of different scattering processes to the mobility and thus carrier transport is additive provided that the scattering mechanisms are independent [64]. Therefore for the above scattering processes, the overall mobility is given by the following relation.

$$\frac{1}{\mu} = \sum_{i=1}^{n} \frac{1}{\mu_i} \tag{3}$$

where μ_i is the mobility due to the ith scattering mechanism. In practice, the conductivity of TCO materials cannot be increased by simultaneously increasing the carrier density and the mobility. Usually, the mobility is observed to saturate and even start to reduce as the carrier density is increased indicating dominant scattering by ionised impurities. Normally, grain boundary scattering is dominant for $N \leq 10^{19}\,\mathrm{cm}^{-3}$ while charge impurity scattering is more significant for $N \geq 10^{19}\,\mathrm{cm}^{-3}$ for ITO and ZnO:Al [1,28,34,66,68]. Recent studies also suggest that for $N > 10^{19}\,\mathrm{cm}^{-3}$, the nature of the scattering differs for both ITO and ZnO:Al as a result of the piezoelectricity of the latter material leading to higher trap densities [66].

Table 1
Deposition methods used to prepare impurity doped In_2O_3 thin films.

Dopant	Method	N ($10^{20}\,\mathrm{cm}^{-3}$)	μ ($\mathrm{cm}^2\mathrm{V}^{-1}\mathrm{s}^{-1}$)	ρ ($10^{-4}\,\Omega$ cm)	T_S (°C)	Ref
Mo	TRE	2.6	130	1.8	350	[57]
	RFMS	3.0	83	2.5	450[a]	[58]
	CSA	7.1	~18.3	4.8	350	[59]
	REHCS	4.1	80.3	1.9	290	[43]
	SP	4.98	~1.72	7.3	450	[60]
	Reactive DCMS	1.9	50	~5.0	350	[61]
	RFM co-sputtering	2.7	99	2.3	450[a]	[39]
	RFM co-sputtering	4.3	65.3	~2.22	550	[40]
	PLD	3.6	250	0.7	500	[41]
	Pulsed DCMS	5.0	77	1.6	500[b]	[9]
Ti	SPD	1.0	120	5.2	500	[42]
	REHCS	4.3	80.6	1.8	300	[43]
	Combinatorial RFMS	2.9	83.3	2.6	500	[44]
	DCMS	2.0	89.5	3.5	300	[45]
	PLD (quartz)	0.8	199	0.98	500	[46]
	RFMS + anneal	3.1	105	1.95	530	[47]
Zr	SP	0.8	170	4.6	500	[42]
	ALD	2.2	76	3.7	500	[52]
	RHCS	4.3	63.3	2.3	250	[43]
	PLD YSZ <111>	1.0	110	5.7	650	[53]
	RFMS	2.9	82	2.6	450	[54]
W	Reactive DCMS	4.0	57	2.7	380	[62]
	DCMS	2.9	73	3.0	300	[49]
	SP	2.4	26	10	525	[63]
	Reactive DCMS	2.8	67	2.8	320	[51]
	PLD (quartz)	~1.5	358	~1.1	500	[50]

N — majority charge carrier density; μ — majority charge carrier mobility; ρ — resistivity and T_S — substrate temperature.
TRE — thermal reactive evaporation; RFMS — RF magnetron sputtering; CSA — channel spark ablation; RHCS — reactive environment hollow cathode sputtering; SP — spray pyrolysis; DCMS — DC magnetron sputtering; PLD pulsed laser deposition and ALD — atomic layer deposition.
[a] Mobility enhanced by post deposition heat treatment.
[b] Substrate temperature estimated to be within 10% of indicated heater temperature.

4.1. Role of crystalline quality and structure

Poor crystalline quality may cause a reduction in the relaxation time and thus mobility as a result of increased point defects, grain boundaries and lattice distortion. Electron transport in n-type semiconductor is facilitated by the vacant s-orbitals of neighbouring cations in the crystal lattice overlapping to form a conduction path. Moreover, if the crystal structure is disrupted by say, a cation vacancy, the spatial spread of the vacant s-orbital around that site is disrupted causing the effective mass of the electron to increase thus reducing its mobility. Therefore, shorter cation–cation bond length and a favourable distribution of the cations are believed to increase the mobility of the electrons in the semiconductor. Early work by Shannon [69] on single crystals in the $CdO–SnO_2–In_2O_3$ family revealed that oxide structures with continuous edge sharing of cation octahedra are essential for conductivity in metal oxides. Later work by Ingram et al. [70] on thin films of the same $CdO–SnO_2–In_2O_3$ family extended this rule to include structures where octahedra share corners. They also classified TCO materials according to the coordination of the cations e.g. ZnO has tetrahedral coordination, while CdO, In_2O_3, SnO_2 and other Cd containing spinel oxides have octahedral coordination. The decrease in both conductivity and mobility was also correlated to a decrease in the octahedral cation density in the structure in the order: CdO (rock salt) > In_2O_3 (bixbyite) > SnO_2 (rutile) [70]. Studies of $ZnSnO_4$ by Mossbauer spectroscopy and X-ray diffraction suggest that the unusually low mobility is a result of disorder on the cation octahedral sites which may disrupt transport between edge sharing cations [71]. Therefore, since high mobility with degenerate doping has only been reported for CdO and In_2O_3 based compounds with octahedrally coordinated cations, the associated cubic structure may also favour high mobility.

4.2. Role of the electronic band structure

The electronic band structure of TCO materials can be studied by theoretical modelling or by measurements of the relaxation time and effective mass as well as the Hall parameters. Owing to the simple structure of CdO, the majority of theoretical electronic band structure studies have been done on this material. Freeman et al. [72,73] have identified three salient features of the electronic band structure of the conduction band of a TCO material which affect the charge carrier transport mechanisms namely, the curvature, the dispersion and the position. A parabolic conduction band minimum ensures a low effective carrier mass of the electrons which promotes high mobility. A study of the $Cd_{1+x}In_{2-2x}Sn_xO_4$ system shows that both the density of states effective mass and the relaxation time increase with N resulting in a cancellation effect such that the mobility is less than expected [74]. In

contrast, the effective carrier mass of IMO was determined as $0.32m_e$ and found to be independent of N implying a parabolic conduction band minimum [58]. A widely dispersed conduction band minimum allows the drift of electrons unimpeded through the crystal structure resulting in a higher relaxation time and thus higher mobility. Electronic band structure calculations of $In_xCd_{1-x}O$ thin films for which mobility up to 91.5 $cm^2V^{-1}s^{-1}$ with $N>10^{20}cm^{-3}$ was measured, revealed an electron effective mass of 0.24–0.26m_e and a broadening of the conduction band edge by hybridization of the Cd 5s and In 5s bands [12]. The calculated effective electron mass agrees with a value of $0.25m_e$ determined by Seebeck measurements [75]. Theoretical studies also suggest that the lowest conduction band of In_2O_3 is split with Sn doping due to the strong hybridization with dopant s-type states and this splitting contributes to both the decrease of the plasma frequency and the mobility of the carriers [73]. In contrast, calculations of the IMO electronic band structure suggest that high mobility is achievable in degenerate In_2O_3:Mo as the d-states of Mo do not hybridize with the s-states of In resulting in m^* similar to undoped In_2O_3 [76].

4.3. Chemical character of impurity dopant element

From the descriptions given above, it can be seen that the choice of elements that induce high mobility in TCO materials has largely been empirical. Few if any studies have been conducted to find the underlying mechanisms for high mobility caused by specific dopants. A series of studies predicted that the mobility of doped In_2O_3 would increase with the Lewis acid strength of the doping element and reported this effect for Ge^{4+}, Si^{4+} and Sn^{4+} [77] as well as for Cu, Ti and Zr [78]. However, the μ of the TCO films studied generally ranged from 45 $cm^2V^{-1}s^{-1}$ to 55 $cm^2V^{-1}s^{-1}$ and in some cases, the films were non-degenerate. In this contribution, we shall attempt to apply the same principles to known degenerately doped In_2O_3 and CdO thin films with mobility >62.5 $cm^2V^{-1}s^{-1}$. The Lewis acid strength L can be calculated using a formula developed by Zhang [79] as follows

$$L = \frac{Z}{r^2} - 7.7\chi_z + 0.8 \quad (4)$$

where r is the ionic radius related to the electrostatic force due to the oxidation state Z of the ion and χ_z is the electronegativity of the element in the respective oxidation state. Using this formula, the Lewis acid strengths of elements that are now known to induce high mobility in In_2O_3 and CdO thin films were compiled in Tables 2 and 3, respectively. All these films presented are highly transparent in the visible and most (where reported) have a high near infra-red region transmission. Generally, it can be seen that the dopants which induce higher mobilities are transition elements which have a higher Lewis acid strength than the host cation.

Table 2
High mobility dopants in In_2O_3 thin films prepared by sputtering on glass substrates except where indicated.

Doping ion	Ionic radius (Å)	Lewis acid strength	N ($10^{20}cm^{-3}$)	μ ($cm^2V^{-1}s^{-1}$)	Ref
H^+	–	–	1.78	130	[32]
Ti^{4+}	0.68	3.064	3.06	104	[47]
Zr^{4+}	0.86	2.043	2.2	76	[52][a]
Nb^{5+}	0.78	2.581	10	65	[81][b]
Gd^{3+}	1.08	0.788	1.74	128	[56][b]
Mo^{6+}	0.62	3.667	2.7	99	[39]
W^{6+}	0.68	3.158	2.9	73	[49]
In^{3+}	0.81	1.026	2.5	60	[82]
Sn^{4+}	0.71	0.228	10.3	43	[16]

The elements are arranged in ascending order of group number and period. The host cation In^{3+} and the more common aliovalent dopant Sn^{4+} have been included for comparison. The values of the ionic radius and Lewis acid strengths have been compiled from calculations by Zhang [79].
[a] Atomic layer deposition ALD at 500 °C.
[b] Pulsed laser deposition on quartz.

Table 3
High mobility doped CdO thin films prepared by MOCVD on glass substrates except where indicated.

Doping ion	Ionic radius (Å)	Lewis acid strength	N ($10^{20}cm^{-3}$)	μ ($cm^2V^{-1}s^{-1}$)	Ref
Sc^{3+}	0.89	1.697	~4.0	~80	[36]
Ti^{4+}	0.68	3.064	23.8	202	[38][a]
Ga^{3+}	0.76	1.167	3	60	[83]
Y^{3+}	1.04	1.465	4.8~	110	[37]
Cd^{2+}	0.99	−0.108	1.5	146	[12]
In^{3+}	0.81	1.026	15	69.2	[12]
Sn^{4+}	0.71	0.228	2	65	[84][a]

The elements are arranged in ascending order of group number and period. The host cation and Cd^{2+} and the more common aliovalent dopant Sn^{4+} have been included for comparison. The values of the ionic radius and Lewis acid strengths have been compiled from calculations by Zhang [79].
[a] Film grown by RF magnetron sputtering.

The lists in Tables 2 and 3 are not exhaustive and have been compiled, where possible, from TCO films prepared by MOCVD or sputtering, respectively, on glass substrates to reduce the influence of the film deposition technique on the mobility values reported. Also, these films may not represent the highest possible mobility achieved by a given dopant. However, most of the dopants listed that induce high mobility in In_2O_3 and CdO are strong Lewis acids compared to Cd^{2+} and In^{3+}, respectively. There are two exceptions in Table 2, namely H^+ and Gd^{3+}. The Lewis acid strength for H^+ has not been calculated because of the difficulty in determining the ionic radius which is anyway expected to be much less than that of In^{3+}. As mentioned previously, H^+ is a shallow donor in most TCO films with a high electron affinity, hydrogen may also passivate defect states in In_2O_3 thus increasing the τ and improving μ [32]. However, the optical properties of H-doped In_2O_3 have not yet been reported. On the other hand, Gd^{3+} has a much higher ionic radius and a lower Lewis acid strength than In^{3+} but corresponds to a high mobility of 128 $cm^2V^{-1}s^{-1}$. Gadolinium belongs to a special group of metals known as Lanthanoids, most of which have a partially filed 4f orbital, lying below group three transition metals in the periodic table and hence may warrant further investigation [80]. While doping CdO by Sn^{4+} and In^{3+} leads to μ~70 $cm^2V^{-1}s^{-1}$, doping using Y^{3+} and Ti^{4+} both transition metal ions results in a drastic increase in μ. We note here that the highest mobility for CdO based material has been observed for a $Cd_{1-x}Sn_xO$ layer grown by pulsed laser deposition on MgO single crystals, as 609 $cm^2V^{-1}s^{-1}$ and $N=4.74\times10^{20}cm^{-3}$.

Sn^{4+} being a non-transition metal ion with a lower Lewis acid strength than In^{3+} will induce a lower mobility in In_2O_3 than the transition elements listed in Table 2. On the other hand, mobility values of <62.5 $cm^2V^{-1}s^{-1}$ with $N>10^{20}cm^{-3}$ have been reported for non-transition metal dopants with high enough Lewis acid strengths such as Sb^{5+} (3.559), Ge^{4+}(3.059) and Si^{4+} (8.098) [77]. According to Wen et al. [77], the high Lewis acid dopants polarise the electronic charge away from the O^{2-} 2p valence band more strongly than weaker Lewis acids, this results in screening of the charge and weakens its activity as a scattering centre hence increasing the mobility. Similarly, the reason for higher mobility in IMO compared to intrinsic In_2O_3 has been explained by Mo suppressing scattering by oxygen interstitials [58]. However, if the Lewis acid is too strong e.g. Ge in In_2O_3, the dopant has a greater affinity to oxygen and may incorporate an excess of oxygen in the lattice which would then limit the μ by the introduction of scattering centres [77].

Originally, the high mobility of IMO was attributed to the higher oxidation state of Mo^{6+} ions that would contribute three extra electrons to the In_2O_3 matrix [57]. Later studies by another group suggested that Mo in IMO exists as both Mo^{4+} and Mo^{6+} for high carrier density and only as Mo^{6+} for films with lower carrier density [85]. However, since other

transition elements with a lower oxidation state such as Ti and Zr, etc show high mobility, a high oxidation state is not necessarily a condition for high mobility. The charge carrier mobility and the visible light transparency of Ti-, Zr-, and Ge-doped In_2O_3 are much higher than that of ITO for the same dopant atomic concentration [78]. A similar comparison of In_2O_3 doped by Sn, Ti and Zr, all of which, can have a oxidation state +4 showed that the electron mobility and the NIR transmission were highest for the transition metal dopants [55]. Though the role of possible multiple valency e.g. of Ti as Ti^{2+} was not considered, these studies asserted that high mobility in In_2O_3 at least is only exhibited for transition metal dopants.

5. Application of high mobility TCO thin films in solar cells

At the front of a solar cell, the TCO layer acts as an electrical contact as well as a window to allow light through to the PV absorber layer. At the back of the cell, the TCO usually acts as an interfacial layer to improve the contact resistance between the PV absorber and a metallic reflector and also as an optical coupling layer by improving the refractive index matching. In bifacial solar cells, the back contact must act both as an electrical contact and as a window layer to let light through the back of the PV absorber layer. Since high photo-conversion efficiency in solar cells requires minimal optical and electrical losses, a TCO layer with sheet resistance of $\leq 10\ \Omega/\square$ and transparency of >80% over the wavelength spectrum useable by the solar cell is mandatory. High mobility TCO materials are especially desirable where a high transparency of >80% is required over a wide spectral range (400–1300 nm) such as in micro-crystalline silicon, CIGS and other multi-junction solar cells.

5.1. Single junction solar cells

High mobility TCO layers can be used as front contact for single junction solar cells in the superstrate configuration because the highest possible process temperatures can be used to optimise the resistivity and transparency. A record efficiency of 16.5% for CdTe solar cells has been achieved using $CdSnO_4$ coated glass in the superstrate configuration [86]. Also, an improved light trapping structure for nano-crystalline silicon solar cells using In_2O_3:Mo layers with a textured ZnO layer can increase the QE for wavelengths exceeding 900 nm compared to cells using ZnO:Al [87]. On the other hand, using In_2O_3:Ti, a relatively low efficiency of 10.7% (compared to state of the art efficiency ~20%) has been obtained for CIGS solar cells in the substrate configuration (glass|Mo|CIGS|ZnO|ITiO) [88]. The reason for this low efficiency is the high series resistance of the cell caused by high resistivity of the ITiO, since the processing of ITiO could not be done at high temperatures, a problem encountered for all other high mobility TCO films as discussed later.

5.2. Bifacial solar cells

Bifacial CIGS thin film solar cells have been prepared on ITiO coated substrates with improved efficiency under rear side illumination as a result of reduced NIR light absorption [89]. However, again here, since the back contact must be highly conductive, a means of processing the HMTCO at low temperature with reasonable conductivity must be developed to realise the full potential of bifacial cells.

5.3. Multi-junction solar cells

The top and intermediate solar cells in a multi-junction configuration require a transparent conducting contact at both the front and back of the cell to ensure efficient transmission of unused light to the underlying lower band gap solar cell. CdTe with an optical band gap ~1.45 eV and amorphous silicon ~1.7 eV are examples of solid state absorber materials suitable for upper junctions in multi-junction solar cells. Also, dye sensitised solar cells (DSC) whose spectral response can be adjusted by varying the TiO_2 nano-particle size or the sensitising dye, are promising candidates for the top junction in a multi-junction solar cells.

CdTe solar cells with a significantly high efficiency of 13.9% have been developed on Cd_2SnO_4 coated glass (μ~53.2 $cm^2V^{-1}s^{-1}$, resistivity $\rho \sim 1.8\times10^{-4}\ \Omega$ cm) while maintaining a NIR transparency of 50% for the entire device [90]. While a high efficiency of the top solar cell is desirable, its full impact on the entire multi-junction solar cell efficiency cannot be realised unless the NIR transparency is improved to ensure adequate current matching with the bottom cells [14]. Improvements in NIR transparency through a TCO|CdTe|TCO device structure to values above 60%, require the use of a HMTCO e.g. Mo- or Ti-doped In_2O_3, at both the front and back sides of the solar cell to reduce parasitic absorption and reflection losses [9]. Fig. 5 shows the NIR transmission spectra of identical CdTe solar cells using all IMO or all ITO contacts. There is a significant gain in NIR transmission when using IMO contacts for a CdTe solar cell that would act as either a top or an intermediate absorber in a multi-junction solar cell. Such a stack requires that the rear side TCO, which has to be prepared at low temperatures over the absorber layers, is sufficiently conductive to prevent losses in the total cell voltage and fill factor which would limit the overall photo-conversion cell efficiency. However, high mobility TCOs have been used to improve the total current of a tandem solar cell consisting of an $Ag(In,Ga)Se_2$ and a $Cu(In,Ga)Se_2$ solar cell [91].

On the other hand, the TCO layers applied at both the front and rear of a dye sensitised solar cell, can be prepared using high process temperatures without the danger of destroying the mesoscopic TiO_2 layers. Taking advantage of this fact, semi-transparent dye sensitised solar cells were prepared using ITiO coated glass for possible application in tandem solar cells [92]. While the NIR transparency increased to 60% compared to DSC devices using FTO coated glass, the efficiency was somewhat lower i.e. 5.8% compared to 8.2%, respectively [92]. The reason for the lower efficiency was the different growth conditions of the TiO_2 interfacial layer on the smoother ITiO films (compared to FTO) and on the elevated resistivity of the ITiO after a sintering step at 450 °C in air required to prepare the porous TiO_2 absorber. A slight improvement in the DSC efficiency to 6.8% could be achieved by adjusting the growth conditions of the dense TiO_2 interfacial layer and by heating the entire stack in vacuum after the sintering step in air [93]. The improvement occurred primarily because of increased fill factor resulting from a lower series resistance due to lower resistivity ITiO layers. Heating the ITiO layer in vacuum, desorbs loosely bound oxygen at the surface creating

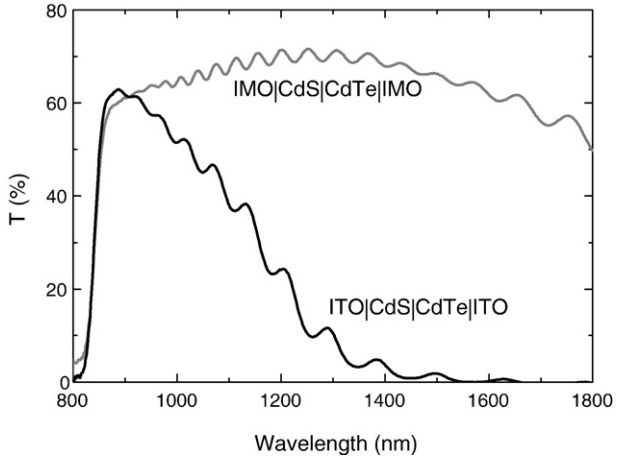

Fig. 5. NIR transmission spectra of two CdTe solar cells, one with all IMO contacts and the other with all ITO contacts.

vacancies and oxygen residing along grain boundaries (if the TCO is slightly porous) thus lowering the depletion barrier along the grain boundaries, increasing the charge carrier density while improving the electron mobility, respectively. This "conduction recovery" phenomenon is used for gas sensor application and was reported in 1977 for $CdIn_2O_4$ [69] and in the early 1980s for SnO_2 [94] and In_2O_3 [95].

6. Challenges and prospects

In 1999, Coutts et al. [96] outlined key areas of basic research to improve the opto-electronic properties of TCO thin films focusing on the development of improved materials which can be easily applied on an industrial scale. While the HMTCO materials reviewed in this article can be prepared with μ of $>62.5\ cm^2V^{-1}s^{-1}$ using sputtering and MOCVD which are well developed deposition techniques for industrial fabrication, some challenges still remain.

6.1. Low mobility in TCO films prepared with low processing temperature

It is desirable to prepare thin films at low temperatures to coat plastic substrates or pre-deposited layers of an opto-electronic device with minimal damage, to reduce the energy input into the manufacturing process and to avoid diffusion of undesirable impurities from the substrate into the TCO films. We note here that all the low resistivity TCO materials with $\mu>62.5\ cm^2V^{-1}s^{-1}$ in Tables 2 and 3 were prepared with deposition temperatures of at least 300 °C. The typical evolution of the ρ, N and μ values of IMO thin films with increasing heater temperature is shown in Fig. 6. The substrate temperature in this case is not more than 10% lower than the heater temperature. These films were prepared by pulsed DC magnetron sputtering from a ceramic In_2O_3:Mo (98:2 wt%) target using argon containing 0.53 vol.% of oxygen at a sputter pressure of 1.0 Pa, with further details reported elsewhere [97]. The resistivity generally reduces as the heater temperature T_H increases from 25 °C to 450 °C then saturates at about $2.0\times10^{-4}\Omega$ cm at 450 °C and 500 °C. The decrease in resistivity is caused by a concurrent increase in N and μ from $0.6\times10^{20}cm^{-3}$ to $4.5\times10^{20}cm^{-3}$ and from $9\ cm^2V^{-1}s^{-1}$ to $73\ cm^2V^{-1}s^{-1}$, respectively.

The observed suppression of mobility to values below $62.5\ cm\ V^{-1}s^{-1}$ at low process temperature of >300 °C, has also been observed by other groups for In_2O_3:Mo [39,43,45,47,85], In_2O_3:Ti [45], In_2O_3:Zr and In_2O_3:Wo [49]. Fig. 7 shows the high resolution Mo 3d XPS spectra for IMO films prepared without intentional substrate heating and with heating to 500 °C which are described in depth elsewhere [97]. In both cases, the molybdenum exists in the oxidation states of +6 and +4 as well as an intermediate oxidation state $+4<x<+6$ [98,99]. The films grown on heated substrates also contain a small amount of elemental Mo. Though the Mo^{6+} state is prevalent in both films, the Mo^{x+} species are much higher in the low temperature film. These Mo^{x+} species are associated with hydroxyls and other complex oxides, such as Mo_4O_{11} [99] which may exist as neutral impurities in the film and thus reduce the mobility by scattering as has also been reported for In_2O_3:Sn films [34,100]. Additionally, the carrier density of the films increases as expected from theory as the Mo^{6+} species exceeds the sum of the remaining Mo species in the film. While this result agrees with some authors [57], other [85] report that the Mo^{4+} species rather than the Mo^{6+} contribute to the conduction electrons in IMO. However, both the maximum values of carrier density $\sim2\times10^{20}cm^{-3}$ and mobility $44\ cm\ V^{-1}s^{-1}$ reported in [85] are less than the corresponding values of $4\times10^{20}cm^{-3}$ and $73\ cm\ V^{-1}s^{-1}$ presented in Fig. 6. Nevertheless, in both cases, the dopant efficiency was lower than 100% indicating that some of the charge carriers could be attributed to oxygen vacancies.

Table 4 lists the electrical and optical characteristics of IMO, IWO, and ITiO thin films grown without intentional substrate heating. It can be seen that regardless of the deposition technique, the IMO films have $\mu<25\ cm^2V^{-1}s^{-1}$ which is slightly less than the value reported for degenerate films of ITO [101,102] and ZnO:Al [17,103] and much less than that for intrinsic In_2O_3 [82,104], all deposited without intentional substrate heating. A similar problem is experienced for films prepared using the other transition elements as dopants for In_2O_3 as listed in Table 4. The cause for low μ for films prepared at low deposition temperatures is not yet fully understood. This is a major

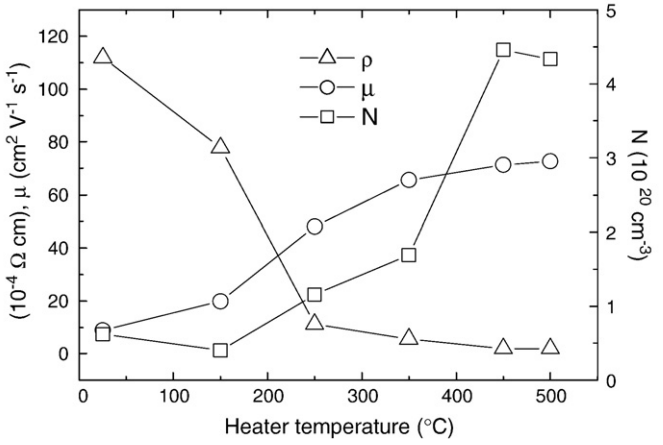

Fig. 6. Resistivity ρ (triangles), Hall mobility μ (circles) and charge carrier density N (squares) of IMO thin films as a function of heater temperature. The lines are to guide the eye.

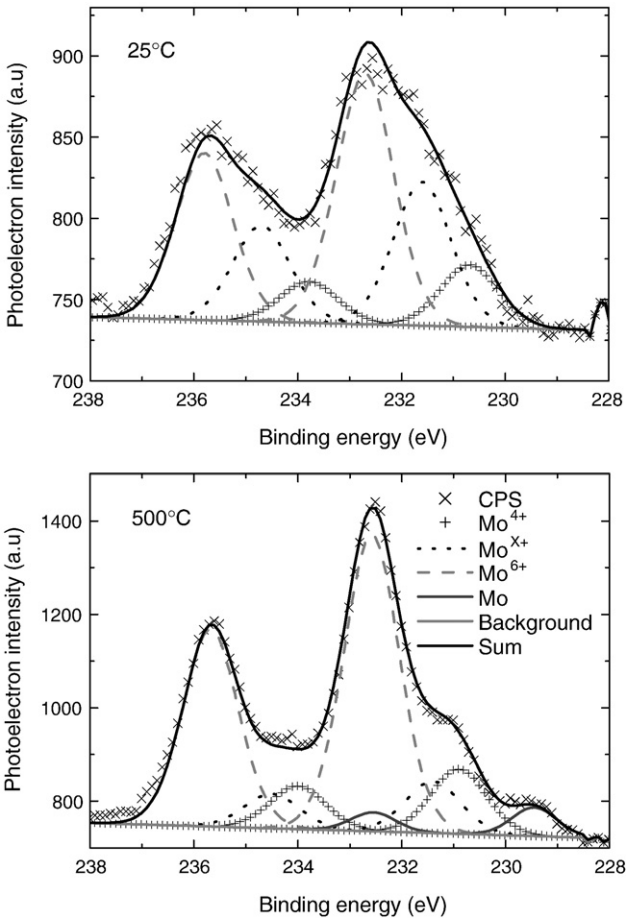

Fig. 7. Mo 3d spectra for In_2O_3:Mo films prepared without intentional heating (25°) and with a heater temperature of 500 °C.

Table 4
A survey of transition element doped In_2O_3 thin films grown without intentional substrate heating.

N (10^{20} cm^{-3})	μ (cm^2/Vs)	ρ ($10^{-4}\Omega$ cm)	d (nm)	T_{VIS} (%)	Target (weight ratio in %)	Method	Ref
0.6	9.0	112	383	75	In_2O_3:Mo (98:2)	Pulsed DCMS	[97]
5.5	22.0	6.1	~140	80	In_2O_3:MoO_3 (95:5)	HDPE	[105]
14.3	14.6	3.6	~140	80	In_2O_3:MoO_3 (99:1)	HDPE	[106]
5.2	20.2	5.9	~130	80	In:Mo (98:2)	Reactive DCMS	[107]
5.2	20.2	5.9	~120	80	"	Reactive DCMS	[108]
1.08	13.6	42.0	300	75	In_2O_3:Mo (95:5)	RF MS	[109]
0.16	19.5	195	~100	80	"	"	[110]
4.16	5.7	26.5	305	18	"	"	[110]
15.0	10.0	5.0	500	–	In_2O_3:TiO_2[a]	DCMS	[45]
0.92	21.0	3.2	~400	–	In_2O_3:WO_3[a]	DCMS	[49]

N — majority charge carrier density; μ — majority charge carrier mobility; ρ — resistivity; d — thickness; T_{VIS} — average visible transmission; DCMS — DC magnetron sputtering; HDPE — high density plasma evaporation; RFMS — RF magnetron sputtering.
[a] Target composition not indicated.

challenge that precludes the preparation of these high mobility films onto heat sensitive substrates.

An interesting development is a significantly high mobility between 50 cm^{2}V^{-1}s^{-1} and 60 cm^{2}V^{-1}s^{-1} that can be obtained in degenerate amorphous Zn-doped In_2O_3 films prepared without substrate heating [111,112]. These films have a relatively high optical transmission in the NIR wavelength region and thus may be an alternative to high mobility TCO materials for coating heat sensitive substrates. It has been proposed that since oxygen vacancies contribute significantly to the conductivity of the IZO thin films, Zn^{2+} substitution on In^{3+} sites does not decrease the carrier density of In_2O_3 films and thus a degenerate carrier density is maintained [104,111]. Further, Zn may increase the density of oxygen vacancies by reducing some of the In–O bonds [104] or by passivating defects caused by interstitial oxygen. The results of the studies mentioned above indicate that the electronic band structure rather than crystalline structure determines the maximum attainable high mobility in TCO materials.

6.2. Inadequate characterisation and analysis methods

One of the major problems in studying the limitations of mobility in TCO films is the difficulty in obtaining sufficiently accurate values of effective mass and relaxation times which are used to determine the dominant scattering mechanisms. Data extracted from optical analysis using Drude's model and the Burstein–Moss shift has to be treated with caution because of the difficulties in measuring the film thickness to a high enough accuracy and assumptions that the conduction band is parabolic, respectively [8,113]. Young et al. [114] described a four coefficient method used to measure the Hall, Seebeck and Nernst coefficients of TCO thin films which can be used to determine the charge carrier density, mobility, the effective electron mass, the scattering mechanisms and relaxation time. However, though Hall measurements are widely used, experimental determination of the Seebeck and Nernst coefficients for these high mobility TCO materials is rarely done, and hence the exact scattering mechanisms limiting the mobility can only be estimated or speculated.

Studies on the electronic transport mechanisms reported for HMTCO films so far seem to be empirical. Theoretical modelling using either computational chemistry or physics methods is a useful tool for calculating and understanding the structure and properties of materials and may even predict hitherto unknown materials with desirable transparent conducting properties. In particular, more insights into the influence of dopant chemistry, dopant concentration, and film structure on the charge carrier transport mechanisms would aid improvements in the resistivity exhibited by these high mobility TCO materials. Developments in electronic band structure calculations may aid in predicting the material behaviour and can help to elucidate limitations to mobility and doping efficiency. For example, a combination of electronic band structure calculations and Seebeck measurements has been used to determine an electron effective mass of Cd_2SnO_4 around $0.25m_e$ [12,75] which is much higher than values of 0.08–0.11m_e and 0.04m_e, determined from the Burstein–Moss shift in the 1970s by Nozik [10] and Haacke [115], respectively. However, most of the reported theoretical electronic band structure calculations for HMTCO have focused on CdO rather than In_2O_3, possibly because of the simplicity of the former's rock salt structure. However since In_2O_3 is less hazardous material and thus more technologically important, more theoretical calculations of the electronic band structure and properties of this material are required to advance the development of TCO materials with improved conductivity.

6.3. Lack of alternative low cost and environmentally benign materials

The high mobility with low resistivity ~$10^{-4}\Omega$ cm values described in the previous sections have only been observed in materials based on In_2O_3 which is rather costly and CdO which is potentially hazardous and may not be acceptable for environmental reasons. Efforts to dope cheaper and environmentally benign materials with transition elements have not yet resulted in higher mobility e.g. ZnO doped with Zr [116], Ti [117], Mo [33], Ta doped SnO_2 [118] and Nb-doped TiO_2 [119]. Also, doping ZnO with hydrogen [120] gives a mobility of ~40 cm^{2}V^{-1}s^{-1} which is comparable with values for Al doping and much less than the value of 130 cm^{2}V^{-1}s^{-1} for H-doped In_2O_3 [32]. It is possible that the wurzite structure of ZnO with tetrahedral coordination is less favourable for electron transport than the cubic structure of CdO and In_2O_3 both of which have an octahedral coordination [70]. In general, for the same dopant element e.g. tin, the mobility of the films increases going from ZnO to In_2O_3 to CdO as Sn inclusion in ZnO causes disorder in the octahedral causing short relaxation times despite the low effective electron mass [71]. Evidently, to achieve high mobility but cheap and non-hazardous TCO materials, alternative dopants or ternary compounds of ZnO, SnO_2 and possibly TiO_2, need to be developed and alternative materials that may not necessarily be oxides should be investigated. Single walled carbon nano-tubes (SWNT) are an emerging p-type transparent conducting material that has low resistivity ~$10^{-4}\Omega$ cm with transparency of >80% over the visible and near infra-red wavelength regions [121]. Promising solar cell efficiencies have been achieved on CIGS [122] and on CdTe [123] using SWNT as transparent contacts. Improvements in SWNT for application in PV should be aimed at reducing the relatively high visible light absorption in films thicker than 100 nm [121–123].

6.4. High resistivity despite higher mobility

Lastly, despite the elevated values of mobility reported, the resistivity of the In_2O_3 and CdO thin films has remained similar to that of state of the art ITO thin films. A lower than expected dopant activation as well as an upper limit for carrier density above which the mobility begins to reduce has been reported for In_2O_3:Mo [58,85,124,125], In_2O_3:W [48,63], In_2O_3:Zr [52,54] and In_2O_3:Ti

[44,45]. For the case of In_2O_3:Mo, it is possible that the reduced dopant activation efficiency of Mo is caused by interstitial oxygen forming neutral complexes with some of the Mo at specific substitutional sites as inferred by some authors [124] and as demonstrated by the XPS measurements discussed in Section 6.1 of this article. Examination of heavily W-doped In_2O_3 thin films by Energy-Filtered Transmission Electron Microscopy revealed segregation of tungsten at the grain boundaries where it is ineffective as a donor [63]. This implies that the transition element dopants limit the mobility through formation of neutral and impurity scattering centres in much the same way as observed for In_2O_3:Sn [34,126]. Theoretical modelling and electronic band structure calculations may be used to understand the limitations to the conductivity of HMTCO films and to predict other eligible dopants. However, for accurate and realistic results, the required calculation time as well as the hardware resources increases with the complexity of the host oxides (especially In_2O_3) and the (transition metal) dopant ions making accurate theoretical calculations difficult.

7. Summary

The literature reviewed in this contribution shows that previously stated limits for mobility in low resistivity TCO films have been exceeded. Several high mobility TCO materials based on In_2O_3 and CdO that combine low resistivity with a high visible and near infra-red optical transmission exist, and the highest mobilities attainable continue to be exceeded. Additionally, these materials can be prepared using industrially mature deposition technologies such as sputtering and chemical vapour deposition without significant degradation of the opto-electronic properties. Several explanations have been given for the high mobility in specific In_2O_3 and CdO based materials but none wholly explain this phenomenon. The application of high mobility TCO layers in various types of thin film solar cells has demonstrated their potential to improve the efficiency of single junction, multi-junction and bifacial solar cells. However, additional aspects such as thermal stability, formation of suitable interfaces with solar cell absorbers and low temperature growth of low resistivity HMTCO films, need to be considered. For large scale production and regardless of the end use, high mobility TCO using alternative cheaper and less hazardous host cation elements than indium and cadmium respectively, are being sought. Other conventional TCO materials based on zinc and tin which are less costly and environmentally benign are still to achieve comparable resistivity and transparency. Additionally, despite the enhanced mobility of HMTCO materials, the resistivity values remain comparable to those of ITO and AZO and the expected reduction to values below $10^{-4}\Omega$ cm is still challenging. Therefore, in the short to medium term, new analysis techniques may be required to learn more about underlying mechanisms for the high mobility in In_2O_3 and CdO based TCO films. In the long term, non-oxide materials may need to be developed while predictions using theoretical methods like electronic band structure calculations may aid in the identification of hitherto unknown high mobility transparent conductors.

Acknowledgement

The authors are grateful to S. Seyrling and S. Buecheler, both of EMPA, Switzerland for the preparation and spectral response measurements of CIGS and CdTe solar cells, respectively. E. Smith of School of Chemistry, Nottingham University, UK is also acknowledged for XPS analysis of the In_2O_3:Mo films. One of the authors, SC, is grateful for a doctoral training grant by the Engineering and Physical Science Research Council, UK.

References

[1] K.L. Chopra, S. Major, D.K. Pandya, Thin Solid Films 102 (1983) 1.
[2] H. Kawazoe, H. Yanagi, K. Ueda, H. Hosono, Mater. Res. Soc. Bull. 25 (2000) 28.
[3] H.L. Hartnagel, A.L. Das, A.K. Jain, C. Jagadish, Semiconducting Transparent Thin Films, Institute of Physics Publishing, Bristol, 1995.
[4] R.G. Gordon, MRS Bull. 25 (2000) 52.
[5] C.G. Granqvist, A. Hultaker, Thin Solid Films 411 (2002) 1.
[6] C.G. Granqvist, Sol. Energy Mater. Sol. Cells 91 (2007) 1529.
[7] T. Minami, Semicond. Sci. Technol. 20 (2005) 35.
[8] T.J. Coutts, D.L. Young, X. Li, MRS Bull. 25 (2000) 58.
[9] S. Calnan, H.M. Uphadhyaya, S. Buecheler, G. Khrypunov, A. Chirila, A. Romeo, R. Hashimoto, T. Nakada, A.N. Tiwari, Thin Solid Films 517 (2009) 2340.
[10] A.J. Nozik, Phys. Rev., B 6 (1972) 453.
[11] A. Tsukazaki, A. Ohtomo, M. Kawasaki, Appl. Phys. Lett. 88 (2006) 152106:1.
[12] A. Wang, J.R. Babcock, N.L. Edelman, A.W. Metz, M.A. Lane, R. Asahi, V.P. Dravid, C.R. Kannewurf, A.J. Freeman, T.J. Marks, Proc. Natl. Acad. Sci. U. S. A. 98 (2001) 7113.
[13] S. Nishiwaki, A. Ennaoui, S. Schuler, S. Siebentritt, M.Ch. Lux-Steiner, Thin Solid Films 431–432 (2003) 296.
[14] T.J. Coutts, J.S. Ward, D.L. Young, K.A. Emery, T.A. Gessert, R. Noufi, Prog. Photovolt: Res. Appl. 11 (2003) 359.
[15] G.J. Exarhos, X.-D. Zhou, Thin Solid Films 515 (2007) 7025.
[16] Y. Shigesato, S. Takaki, T. Haranoh, J. Appl. Phys. 71 (1992) 3356.
[17] K. Ellmer, J. Phys. D: Appl. Phys. 33 (2000) R17.
[18] M. Bender, J. Trube, J. Stollenwerk, Thin Solid Films 354 (1999) 100.
[19] M. Lorenz, E.M. Kaidashev, H. von Wenckstern, V. Riede, C. Bundesmann, D. Spemann, G. Benndorf, H. Hochmuth, A. Rahm, H.-C. Semmelhack, M. Grundmann, Solid State Electron. 47 (2003) 2205.
[20] H. Ohta, M. Orita, M. Hirano, H. Tanji, H. Kawazoe, H. Hosono, Appl. Phys. Lett. 76 (2000) 2740.
[21] M. Yan, M. Lane, C.R. Kannewurf, R.P.H. Chang, Appl. Phys. Lett. 78 (2001) 2342.
[22] C. Agashe, O. Kluth, J. Hüpkes, U. Zastrow, B. Rech, M. Wüttig, J. Appl. Phys. 95 (2004) 1911.
[23] I.A. Rauf, J. Mater. Sci. Lett. 12 (1993) 1902.
[24] I.A. Rauf, Mater. Lett. 18 (18) (1993) 123.
[25] R. Dingle, H.-L. Störmer, A.C. Gossard, W. Wiegmann, Appl. Phys. Lett. 33 (1978) 665.
[26] J.J. Robbins, C.A. Wolden, Appl. Phys. Lett. 83 (2003) 3933.
[27] D.J. Cohen, S.A. Barnett, J. Appl. Phys. 98 (2005) 053705.
[28] K. Ellmer, G. Vollweiler, Thin Solid Films 496 (2006) 1104.
[29] T. Suzuki, T. Yamazaki, H. Oda, J. Mater. Sci. Lett. 23 (1988) 3026.
[30] Ç. Kiliç, A. Zunger, Appl. Phys. Lett. 81 (2002) 73.
[31] S.H. Keshmiri, M. Rezaee-Roknabadi, S. Ashok, Thin Solid Films 413 (2002) 167.
[32] T. Koida, H. Fujiwara, M. Kondo, J. Non-Cryst. Solids 354 (2008) 2805.
[33] J.N. Duenow, T.A. Gessert, D.M. Wood, T.M. Barnes, M. Young, B. To, T.J. Coutts, J. Vac. Sci. Technol., A 25 (2007) 955.
[34] G. Frank, H. Köstlin, Appl. Phys. A 27 (1982) 197.
[35] K. Utsumi, H. Iigusa, R. Tokumaru, P.K. Song, Y. Shigesato, Thin Solid Films 445 (2003) 229.
[36] S. Jin, Y. Yang, J.E. Medvedeva, J.R. Ireland, A.W. Metz, J. Ni, C.R. Kannewurf, A.J. Freeman, T.J. Marks, J. Am. Chem. Soc 126 (2004) 13787.
[37] Y. Yang, S. Jin, J.E. Medvedeva, J.R. Ireland, A.W. Metz, J. Ni, M.C. Hersam, A.J. Freeman, T.J. Marks, J. Am. Chem. Soc 127 (2005) 8796.
[38] B. Saha, R. Thapa, K.K. Chattopadhyay, Solid State Commun. 145 (2008) 33.
[39] N. Yamada, T. Tatejima, H. Ishizaki, T. Nakada, Jpn. J. Appl. Phys. 45 (2006) L1179.
[40] M.F.A.M. van Hest, M.S. Dabney, J.D. Perkins, D.S. Ginley, Thin Solid Films 496 (2006) 70.
[41] R.K. Gupta, K. Ghosh, S.R. Mishra, P.K. Kahol, Appl. Surf. Sci. 254 (2008) 4018.
[42] R. Groth, Phys. Status Solidi 14 (1966) 69.
[43] A.E. Delahoy, S.Y. Guo, J. Vac. Sci. Technol. A23 (2005) 1215.
[44] M.F.A.M. van Hest, M.S. Dabney, J.D. Perkins, D.S. Ginley, M.P. Taylor, Appl. Phys. Lett. 87 (2005) 032111:1.
[45] Y. Abe, N. Ishiyama, J. Mater. Sci. 41 (2006) 7580.
[46] R.K. Gupta, K. Ghosh, S.R. Mishra, P.K. Kahol, Appl. Surf. Sci. 253 (2007) 9422.
[47] R. Hashimoto, Y. Abe, T. Nakada, Appl. Phys. Express 1 (2008) 015002.
[48] P.F. Newhouse, C.-H. Park, D.A. Keszler, J. Tate, P.S. Nyholm, Appl. Phys. Lett. 87 (2005) 1121081.
[49] Y. Abe, N. Ishiyama, Mater. Lett. 61 (2007) 566.
[50] R.K. Gupta, K. Ghosh, S.R. Mishra, P.K. Kahol, Appl. Surf. Sci. 254 (2008) 1661.
[51] M. Yang, J. Feng, G. Li, Q. Zhang, J. Cryst. Growth 310 (2008) 3474.
[52] T. Asikainen, M. Ritala, M. Leskelä, Thin Solid Films 440 (2003) 152.
[53] T. Koida, M. Kondo, Appl. Phys. Lett. 89 (2006) 082104:1.
[54] T. Koida, M. Kondo, J. Appl. Phys. 101 (2007) 063705:1.
[55] T. Koida, M. Kondo, J. Appl. Phys. 101 (2007) 063713:1.
[56] R.K. Gupta, K. Ghosh, S.R. Mishra, P.K. Kahol, Thin Solid Films 516 (2008) 3204.
[57] Y. Meng, X. Yang, H. Chen, J. Shen, Y. Jiang, Z. Zhang, Z. Hua, Thin Solid Films 394 (2001) 219.
[58] Y. Yoshida, D.M. Wood, T.A. Gessert, T.J. Coutts, Appl. Phys. Lett. 84 (2004) 2097.
[59] L. Huang, X.-F. Li, Q. Zhang, W.-N. Miao, L. Zhang, X.-J. Yan, Z.-J. Zhang, H. Z.-Y., J. Vac. Sci. Technol., A 23 (2005) 1350.
[60] D.J. Seo, S.H. Park, Physica. B 357 (2005) 420.
[61] X. Li, W. Miao, Q. Zhang, L. Huang, Z. Zhang, Z. Hua, J. Mater. Res. 20 (2005) 1404.
[62] X. Li, Q. Zhang, W. Miao, L. Huang, Z. Zhang, Thin Solid Films 515 (2006) 2471.
[63] D.R. Acosta, A.I. Martínez, Thin Solid Films 515 (2007) 8432.
[64] M. Lundstrom, Fundamentals of Carrier Transport, Cambridge University Press, Cambridge, 2000.
[65] R. Clanget, Appl. Phys. 2 (1973) 247.
[66] K. Ellmer, R. Mientus, Thin Solid Films 516 (2008) 5829.
[67] K. Ellmer, J. Phys. D: Appl. Phys. 34 (2001) 3097.
[68] H.L. Hartnagel, A.L. Das, A.K. Jain, C. Jagadish, Semiconducting Transparent Thin Films, Institute of Physics Publishing, Bristol, 1995.

[69] R.D. Shannon, J.L. Gillson, R.J. Bouchard, J. Phys. Chem. Solids 38 (1977) 877.
[70] B.J. Ingram, G.B. Gonzalez, D.R. Kammler, M.I. Bertoni, T.O. Mason, J. Electroceram. 13 (2004) 167.
[71] D.L. Young, D.L. Williamson, T.J. Coutts, J. Appl. Phys. 91 (2002) 1464.
[72] A.J. Freeman, K.R. Poeppelmeier, T.O. Mason, R.P.H. Chang, T.J. Marks, MRS Bull. 25 (2000) 45.
[73] O.N. Mryasov, A.J. Freeman, Phys. Rev., B 64 (2001) 233111.
[74] D.R. Kammler, T.O. Mason, D.L. Young, T.J. Coutts, D. Ko, K.R. Poeppelmeier, D.L. Williamson, J. Appl. Phys. 90 (2001) 5979.
[75] T. Pisarkiewicz, K. Zakrzewska, E. Leja, Thin Solid Films 153 (1987) 479.
[76] J.E. Medvedeva, Phys. Rev. Lett. 97 (2006) 086401.
[77] S.J. Wen, G. Campet, J. Portier, G. Couturier, J.B. Goodenough, Mater. Sci. Eng. B14 (1992) 115.
[78] S.J. Wen, G. Campet, Act. Passive Electron. Compon. 15 (1993) 79.
[79] Y. Zhang, Inorg. Chem. 21 (1982) 3889.
[80] IUPAC Periodic Table of the Elements, (22 June 2007) http://www.iupac.org/reports/periodic_table/.
[81] R.K. Gupta, K. Ghosh, R. Patel, S.R. Mishra, P.K. Kahol, Mater. Chem. Phys. 112 (2008) 136.
[82] H. Nakazawa, Y. Ito, E. Matsumoto, K. Adachi, N. Aoki, Y. Ochiai, J. Appl. Phys. 100 (2006) 093706:1.
[83] S. Jin, Y. Yang, J.E. Medvedeva, L. Wang, S. Li, N. Cortes, J.R. Ireland, A.W. Metz, J. Ni, M.C. Hersam, A.J. Freeman, T.J. Marks, Chem. Mater. 20 (2008) 220.
[84] X. Wu, W.P. Mulligan, T.J. Coutts, Thin Solid Films 286 (1996) 274.
[85] Y. Yoshida, T.A. Gessert, C.L. Perkins, T.J. Coutts, J. Vac. Sci. Technol., A 21 (2003) 1092.
[86] X. Wu, J.C. Keane, R.G. Dhere, C. DeHart, A. Duda, T.A. Gessert, S. Asher, D.H. Levi, P. Sheldon, 17th European Photovoltaic Solar Energy Conference, Munich, Germany, 22–26 October 2001, 2001, p. 995.
[87] J.A. Anna Selvan, A.E. Delahoy, S. Guo, Y.-M. Li, Sol. Energy Mater. Sol. Cells 90 (2006) 3371.
[88] A.E. Delahoy, L. Chen, M. Akhtar, B. Sang, S. Guo, Sol. Energy 77 (2004) 785.
[89] T. Nakada, T. Miyano, R. Hashimoto, Y. Kanda, T. Mise, 22nd European Photovoltaic Solar Energy Conference, Milan, Italy, 2007, p. 1870.
[90] X. Wu, J. Zhou, A. Duda, J.C. Keane, T.A. Gessert, Y. Yan, R. Nouli, Prog. Photovolt: Res. Appl. 14 (2006) 471.
[91] S.K.T. Nakada, Y. Kuromiya, R. Arai, Y. Ishii, N. Kawamura, H. Ishizaki, N. Yamada, Conference Record of the 2006 IEEE 4th World Conference on Photovoltaic Energy Conversion, Hawaii, USA, 2006, p. 400.
[92] J.W. Bowers, H.M. Upadhyaya, S. Calnan, T. Hashimoto, T. Nakada, A.N. Tiwari, Prog. Photovolt. Res. Appl. 17 (2008) 265.
[93] J.W. Bowers, H.M. Upadhyaya, S. Calnan, S.J. Watson, R. Hashimoto, T. Nakada, A.N. Tiwari, Proc. 23rd European Photovoltaic Solar Energy Conf., Valencia, Spain, 2008, p. 748.
[94] E. Shanthi, A. Banerjee, V. Dutta, K.L. Chopra, Thin Solid Films (1980) 237.
[95] A. Gupta, P. Gupta, V.K. Srivastava, Thin Solid Films 123 (1985) 325.
[96] T.J. Coutts, J.D. Perkins, D.S. Ginley, T.O. Mason, 195th Meeting of the Electrochemical Society, Seattle, Washington, May 2–6, 1999, August 1999.
[97] S. Calnan, E. Smith, S.E. Dann, H.M. Uphadyaya, A.N. Tiwari, (in press).
[98] C.D. Wagner, Spectroscopy 1 (1990) 595.
[99] NIST X-ray Photoelectron Spectroscopy Database, (2003) http://srdata.nist.gov/xps/.
[100] O. Warschkow, D.E. Ellis, G.B. González, T.O. Mason, J. Am. Ceram. Soc. 86 (2003) 1707.
[101] C. Guillén, J. Herrero, J. Appl. Phys. 101 (2007) 073514.
[102] J.R. Bellingham, W.A. Phillips, C.J. Adkins, J. Phys.: Condens. Matter. 2 (1990) 6201.
[103] M. Berginski, J. Hüpkes, M. Schulte, G. Schöpe, H. Stiebig, B. Rech, M. Wuttig, J. Appl. Phys. 101 (2007) 074903:1.
[104] B.B. Yaglioglu, Y.-J. Huang, H.-Y. Yeom, D.C. Paine, Thin Solid Films 496 (2006) 89.
[105] S.-Y. Sun, J.-L. Huang, D.-F. Lii, Thin Solid Films 469–470 (2004).
[106] S.-Y. Sun, J.-L. Huang, D.-F. Lii, J. Mater. Res. 20 (2005) 248.
[107] X. Li, W. Miao, Q. Zhang, Li Huang, Z. Zhang, Z. Hua, Semicond. Sci. Technol. 20 (2005) 835.
[108] W.-N. Miao, X.-F. Li, Q. Zhang, L. Huang, Z.-J. Zhang, L. Zhang, X.-J. Yan, Thin Solid Films 500 (2006) 70.
[109] E. Elangovan, R. Martins, E. Fortunato, Thin Solid Films 515 (2007) 8549.
[110] E. Elangovan, A. Marques, A.S. Viana, R. Martins, E. Fortunato, Thin Solid Films 516 (2008) 1359.
[111] R. Martins, P. Barquinha, A. Pimentel, L. Pereira, E. Fortunato, Phys. Status Solidi A202 (2005) R95.
[112] E. Fortunato, A. Pimentel, A. Gonçalves, A. Marques, R. Martins, Thin Solid Films 502 (2006) 104.
[113] I. Hamberg, C.G. Granqvist, J. Appl. Phys. 60 (1986) R123.
[114] D.L. Young, T.J. Coutts, V.I. Kaydanov, Rev. Sci. Instrum. 71 (2000) 462.
[115] G. Haacke, W.E. Mealmaker, L.A. Siegel, Thin Solid Films 55 (1978) 67.
[116] H. Kim, J.S. Horwitz, W.H. Kim, S.B. Qadri, Z.H. Kafafi, Appl. Phys. Lett. 83 (2003) 3809.
[117] Y.-M. Lu, C.-M. Chang, S.-I. Tsai, T.-S. Wey, Thin Solid Films 447–448 (2004) 56.
[118] H. Toyosaki, M. Kawasaki, Y. Tokura, Appl. Phys. Lett. 93 (132109) (2008) 1.
[119] Y. Furubayashi, T. Hitosugi, Y. Yamamoto, Y. Hirose, G. Kinoda, K. Inaba, T.H.T. Shimada, Thin Solid Films 496 (2006) 157.
[120] L.-Y. Chen, W.-H. Chen, J.-J. Wang, F.C.-N. Hong, Y.-K. Su, Appl. Phys. Lett. 85 (2004) 5628.
[121] Z. Wu, Z. Chen, X. Du, J.M. Logan, J. Sippel, M. Nikolou, K. Kamaras, J.R. Reynolds, D.B. Tanner, A.F. Hebard, A.G. Rinzler, Science 305 (2004) 1273.
[122] T.B.M. Contreras, J. van de Lagemaat, G. Rumbles, T.J. Coutts, C. Weeks, P. Glatkowski, I. Levitsky, J. Peltola, Proc. 4th World Conference on Photovoltaic Energy Conversion, Hawaii, USA, 2006, p. 428.
[123] T.M. Barnes, X. Wu, J. Zhou, A. Duda, J. van de Lagemaat, T.J. Coutts, C.L. Weeks, D.A. Britz, P. Glatkowski, Appl. Phys. Lett. 90 (2007) 243503:1.
[124] C. Warmsingh, Y. Yoshida, D.W. Readey, C.W. Teplin, J.D. Perkins, P.A. Parilla, L.M. Gedvilas, B.M. Keyes, D.S. Ginley, J. Appl. Phys. 95 (2004) 3831.
[125] Y. Yoshida, C. Warmsingh, T.A. Gessert, D.L. Young, D.M. Wood, J.D. Perkins, D.S. Ginley, T.J. Coutts, Proc. 3rd World Conference on Photovoltaic Energy Conversion, Osaka, Japan., 2003, p. 34.
[126] M. Kamei, H. Enomoto, I. Yasui, Thin Solid Films 392 (2001) 265.